given by (6) can successfully shorten the settling time of the tracking control at different operation speeds. In our experimental setup the settling time is in the range of $0.50 \sim 0.65$ s for the conveyor belt running between $9.43 \sim 26.60$ cm/s. As we have seen, this is a great improvement in the tracking control compared with that where no special care is taken to compensate for the feedback signal when the sensor is operating in the saturated region. Again, the advantage of the predictive method becomes more evident as the speed of the conveyor becomes faster.

VI. Conclusion

This paper presents a position tracking control for use in production lines. The concept of synchronous tracking and working is of great industrial applicability, and has positive effects on shortening manufacturing time and increasing manufacturing efficiency. An H^∞ robust controller has been implemented successfully in an experimental setup with a robot arm sitting on the working table. The design problem of sensor output saturation was successfully dealt with by using a predictive method while the sensor is operating in the saturated range.

In our experiments only one processing mechanism was used at a time. It might be possible, however, to use two or more simultaneously tracking and working devices in conjunction, and thereby further increase productivity.

References

[1] B. A. Francis, *A Course in H^∞ Control Theory*. Berlin: Springer-Verlag, 1987.

[2] H. Hanselmann, "Implementation of digital controllers—A survey," *Automatica*, vol. 23, pp. 7–32, 1987.

[3] C. H. Lee, "Performance improvement of a synchronous tracking control system," Master's thesis, National Cheng Kung University, Tainan, Taiwan, 1993.

[4] R. A. Hyde and K. Glover, "A comparison of different scheduling techniques for H^∞ controllers," *Trans. Inst. Meas. Contr.*, vol. 13, pp. 227–232, 1991.

[5] D. McFarlane and K. Glover, "A loop shaping design procedure using H^∞ synthesis," *IEEE Trans. Automat. Contr.*, vol. 37, pp. 759–769, 1992.

[6] ——, *Robust Controller Design Using Normalized Coprime Factor Plant Descriptions*. Berlin: Springer-Verlag, 1990.

[7] I. Postlethwaite, M. C. Tsai, and D. W. Gu "Weighting function selection in H^∞ design," in *Proc. IFAC Conf.*, Tallinn, Estonia, 1990, vol. 3, pp. 127–132.

[8] M. G. Safonov, A. J. Laub, and G. L. Hartmann, "Feedback properties of multivariable systems: The role and use of the return difference matrix," *IEEE Trans. Automat. Contr.*, vol. AC-26, pp. 47–65, 1981.

[9] D. J. Walker and I. Postlethwaite, "Discrete time H^∞ control laws for a high performance helicopter," in *Proc. 30th IEEE Conf. Decision and Control*, Brighton, England, 1991, vol. 1, pp. 128–129.

[10] OMRON Inc., *The OMRON Handbook: Best Control Machines*, 11th ed., Japan, 1992.

Approximate Inverse Dynamics and Passive Feedback for Flexible Manipulators with Large Payloads

Christopher J. Damaren

***Abstract*— A derivation is presented of an approximate form of the dynamics governing a structurally flexible manipulator carrying a massive payload at its end-effector. An output called the μ-tip rate which incorporates end-effector and elastic motions is introduced. The input-output mapping relating a transformed version of the joint torques to the μ-tip rates is shown to be passive for large payloads. A feedforward torque strategy is developed which preserves the passivity property in the error dynamics and a suitable Lyapunov function is used to demonstrate global asymptotic stability of the tracking provided by a PD law. Implementation of the controllers without measurements of the elastic coordinates and rates is shown to be possible. Simulation studies of a six DOF manipulator with flexible links, modeled after the Shuttle Remote Manipulator System, demonstrate excellent tracking in all six Cartesian end-effector coordinates, even for payloads with modest mass properties. A major conclusion is that some of the problems normally associated with lack of collocation in flexible manipulators can be surmounted when large (massive) payloads are involved.**

I. Introduction

In the last two decades, a coherent theory of control for rigid robot manipulators has emerged. Globally stable trajectory tracking has been demonstrated with respect to "exact" nonlinear models of rigid robot dynamics. The tutorial paper [1], while primarily focusing on adaptive control, presents a useful subdivision of globally stabilizing controllers into those based on feedback linearization and those which exploit the concept of passivity. The success of controllers in the latter group can be attributed to the collocation of torque actuation and joint rate sensing which ensures passivity in the open-loop forward dynamics operator [2].

General mechanical systems possessing collocation of force inputs and rate outputs such as flexible space structures [3] exhibit passivity on account of the energy balance between the system Hamiltonian and the work done by inputs and dissipative influences. The major importance of this concept in controller synthesis arises from the Passivity Theorem (see [4] for example) which states that the feedback interconnection of a passive system and a strictly passive one is input-output stable. The recognition that passive systems possess a natural Lyapunov function in the form of the storage function [5], [6] leads to the more common notion of Lyapunov stability. For passive mechanical systems, the storage function can usually be identified with the Hamiltonian which has been fully exploited in controlling rigid manipulators. In the case of structurally flexible manipulators, the passivity of the map relating the applied torques to the joint rates persists given the physical collocation. However, this knowledge is less strategic than in the rigid case since the true goal is usually tracking of a prescribed end-effector trajectory.

In general, the map from joint torques to end-effector rates is not passive for a flexible arm. In the case of a single flexible link, it is well-known that the transfer function from joint torque to tip rate is nonminimum phase. As noted in [7], the forward dynamics operator in the multilink case exhibits the nonlinear analog of the nonminimum phase property in linear systems, namely instability

Manuscript received February 11, 1994; revised January 1, 1995.

The author is with the Department of Mechanical Engineering, University of Canterbury, Christchurch, New Zealand.

Publisher Item Identifier S 1042-296X(96)01066-4.

1042–296X/96$05.00 © 1996 IEEE

of the so-called zero dynamics. Hence, inversion of the forward dynamics map from joint torque to generalized end-effector rates leads to a noncausal solution which was obtained in [8] using a frequency domain approach. Given these difficulties noted, many approaches to the control of flexible manipulators have employed joint-based control schemes. The joint space inversion strategy in [9] yielded stabilization of the joint trajectory errors and inherent structural damping provided stability of the elastic coordinates.

Given the desirability of the passivity and/or minimum phase properties, some research has concentrated on modifying the output of robotic systems in order to realize this property. Wang and Vidyasagar [9], [10] have introduced the reflected tip position for a single flexible link. The tip position was taken as the sum of a rigid contribution from the joint angle and an elastic contribution from the tip deflection. They defined the reflected tip position as the rigid portion *less* the elastic part and showed numerically that the transfer function from root torque to reflected tip rate is passive. This was rigorously demonstrated by Pota and Vidyasagar [11] using the properties of the pinned-free modes of the link. Other well-behaved transfer functions were studied in [12]. Minimum phase (but not passive) behavior of a transfer function employing the tip position was demonstrated in [13] as the mass distribution was shifted toward the link tip. The authors of [14] have considered the effect of payload mass on the control of a single flexible link.

The above works furnished the original motivation for our approach which was initiated in [15]. There, the modified output idea was extended to the case of a general, nonredundant, flexible manipulator attached to a free spacecraft and carrying a payload. The linearized dynamics in the vicinity of a constant setpoint were formulated and the transfer matrix relating suitably defined inputs and outputs was shown to be positive real—equivalent to passivity for linear time-invariant systems—when the payload was very massive. This situation is well-represented in space-based manipulation scenarios where necessarily flimsy robots currently maneuver large satellites and are presently being developed for Space Station assembly.

The contributions of the present work are as follows. The approximate (nonlinear) dynamics (AD) governing a flexible manipulator when the payload is much more massive than the manipulator are developed in Section III. Building on [15], we establish the passivity properties inherent in the AD using a special output involving the end-effector rates. A feedforward strategy based on the AD is formulated which preserves the passivity property in the tracking error dynamics. Feedback strategies using the modified output are developed in Section V and Lyapunov analysis is used to demonstrate global asymptotic stability for the end-effector tracking errors. The previous ideas are validated using an "exact" simulation of a six rigid DOF model of the Space Shuttle Remote Manipulator System with link flexiblity. An attempt is made to establish the validity of the approach over a range of payload mass properties. Consideration will be given to controllers which do not require direct sensing of the elastic coordinates or their rates.

II. System Description

The system under consideration consists of a chain of bodies, $\{\mathcal{B}_0, \cdots, \mathcal{B}_{N+1}\}$, with reference frame F_n in $\mathcal{B}_n$. The frame F_0 represents a fixed inertial reference frame ($\mathcal{B}_0$ is fixed). The bodies are taken to be rigid or flexible and interconnected with single DOF revolute joints; the joint angles are $\boldsymbol{\theta} \triangleq \text{col}\{\theta_n(t)\}$, $n \in [1, N]$, and the ensemble of elastic coordinates describing the flexible deformations will be designated $\mathbf{q}_e(t) \triangleq \text{col}\{\mathbf{q}_{n,e}\}$ where $\mathbf{q}_{n,e} \triangleq \text{col}\{q_{n\alpha}\}$ are the expansion coefficients in the spatial discretization of link n. Cantilevered to the end of $\mathcal{B}_N$ is a rigid payload, $\mathcal{B}_{N+1}$. Hence, its body-fixed frame F_{N+1} locates the end-effector and it will be assumed that $\mathcal{B}_{N+1}$ is significantly more massive than the link bodies, $\{\mathcal{B}_1, \cdots, \mathcal{B}_N\}$.

The motion equations of the system described above are of the standard form

$$\boldsymbol{M}(\mathbf{q})\ddot{\mathbf{q}} + \boldsymbol{D}\dot{\mathbf{q}} + \boldsymbol{K}\mathbf{q} = \boldsymbol{B}\tau(t) + \mathbf{f}_{non}(\mathbf{q}, \dot{\mathbf{q}}), \quad \mathbf{q} \triangleq \text{col}\{\theta, \mathbf{q}_e\}. \tag{1}$$

$\boldsymbol{M} = \boldsymbol{M}^T > 0$ is the mass matrix, $\tau(t)$ is a column of applied joint torques, and $\mathbf{f}_{non}$ are nonlinear inertial forces which are quadratic in $\dot{\mathbf{q}}$. If it is assumed that the elastic coordinates are generated using clamped-free boundary conditions for each link, then the damping, stiffness, and input matrices can be further partitioned as $\boldsymbol{D} = \text{diag}\{\mathbf{O}, \boldsymbol{D}_{ee}\}$, $\boldsymbol{K} = \text{diag}\{\mathbf{O}, \boldsymbol{K}_{ee}\}$, and $\boldsymbol{B}^T = [\mathbf{1} \ \ \mathbf{O}]$. The matrices $\boldsymbol{D}_{ee}$ and $\boldsymbol{K}_{ee}$ are positive-definite and for simplicity it will be assumed that they are constant. However, nonlinear effects such as geometric stiffening can be captured through the use of nonlinear strain displacement relations which leads to a quadratic dependence on $\mathbf{q}_e$ in $\boldsymbol{K}_{ee}$. Letting T and V be the kinetic and strain energies respectively, the Hamiltonian for the system and its rate satisfy

$$H_0 = T + V = \tfrac{1}{2}\dot{\mathbf{q}}^T\boldsymbol{M}(\mathbf{q})\dot{\mathbf{q}} + \tfrac{1}{2}\mathbf{q}_e^T\boldsymbol{K}_{ee}\mathbf{q}_e, \quad \dot{H}_0 = \tau^T\dot{\boldsymbol{\theta}} - \dot{\mathbf{q}}_e^T\boldsymbol{D}_{ee}\dot{\mathbf{q}}_e \tag{2}$$

i.e., H_0 evolves according to the work done by τ and the dissipative influences.

The forward kinematics describing the end-effector position and orientation can be summarized by constructing $\mathbf{C}_{N+1,0}(\boldsymbol{\theta}, \mathbf{q}_e)$, the rotation matrix from F_0 to F_{N+1}, and $\mathbf{r}_{0,N+1}(\boldsymbol{\theta}, \mathbf{q}_e)$, the position of F_{N+1} with respect to F_0 expressed in the latter frame. The generalized Cartesian position of the payload, $\boldsymbol{\rho}(t)$, is a 6-tuple whose upper half consists of the position coordinates, i.e., $\mathbf{r}_{0,N+1}$, and whose bottom half contains 3 integrable attitude coordinates (Euler angles) parametrizing the rotation matrix $\mathbf{C}_{N+1,0}$. The Cartesian velocities of the end-effector can be related to the joint and elastic coordinates rates

$$\dot{\boldsymbol{\rho}} = \boldsymbol{J}_\theta(\boldsymbol{\theta}, \mathbf{q}_e)\dot{\boldsymbol{\theta}} + \boldsymbol{J}_e(\boldsymbol{\theta}, \mathbf{q}_e)\dot{\mathbf{q}}_e \tag{3}$$

where $\boldsymbol{J}_\theta$ shall be referred to as the rigid Jacobian and $\boldsymbol{J}_e$ as the elastic Jacobian. The construction of the two Jacobian matrices given the geometric and elastic link properties is described in the companion work [15]. The matrix $\boldsymbol{J}_\theta(\boldsymbol{\theta}, \mathbf{0})$ can be identified with the Jacobian of the corresponding rigid manipulator.

Let $\mathbf{v}_{N+1}$ and $\boldsymbol{\omega}_{N+1}$ denote the absolute velocity and angular velocity of $\mathcal{B}_{N+1}$ expressed in F_{N+1}. They can be collected into a single generalized velocity vector $\boldsymbol{v}_t \triangleq \text{col}\{\mathbf{v}_{N+1}, \boldsymbol{\omega}_{N+1}\}$ which satisfies

$$\boldsymbol{v}_t = \boldsymbol{P}_t(\boldsymbol{\rho})\dot{\boldsymbol{\rho}} = \widehat{\boldsymbol{J}}_\theta\dot{\boldsymbol{\theta}} + \widehat{\boldsymbol{J}}_e\dot{\mathbf{q}}_e, \ \boldsymbol{P}_t = \text{diag}\{\mathbf{C}_{N+1,0}(\boldsymbol{\rho}), \mathbf{S}_{N+1,0}(\boldsymbol{\rho})\} \tag{4}$$

where $\mathbf{S}_{N+1,0}$ is the configuration-dependent matrix mapping Euler rates into angular velocity. The hatted Jacobians $\widehat{\boldsymbol{J}}_\theta \triangleq \boldsymbol{P}_t\boldsymbol{J}_\theta$ and $\widehat{\boldsymbol{J}}_e \triangleq \boldsymbol{P}_t\boldsymbol{J}_e$ yield velocities in the payload coordinate system. We also define

$$\boldsymbol{v}_t^\otimes \triangleq \begin{bmatrix} \boldsymbol{\omega}_{N+1}^\times & \mathbf{O} \\ \mathbf{v}_{N+1}^\times & \boldsymbol{\omega}_{N+1}^\times \end{bmatrix}, \quad \boldsymbol{v}_t^T\boldsymbol{v}_t^\otimes = \mathbf{0} \tag{5}$$

which will be used extensively in the next section. The notation $(\cdot)^\times$ denotes the 3×3 skew-symmetric matrix used to implement the vector cross product.

A passive transfer function was obtained for $N = 1$ in [9] by introducing the reflected tip position. This approach can be generalized by separating $\dot{\boldsymbol{\rho}}$ into contributions from the joint motion and those due to the link deformations. To this end, define the *μ-tip*

rate by

$$\dot{\boldsymbol{\rho}}_\mu \triangleq \boldsymbol{J}_\theta\dot{\boldsymbol{\theta}} + \mu\boldsymbol{J}_e\dot{\mathbf{q}}_e = \mu\dot{\boldsymbol{\rho}} + (1-\mu)\boldsymbol{J}_\theta(\boldsymbol{\theta},\mathbf{q}_e)\dot{\boldsymbol{\theta}} = \dot{\boldsymbol{\rho}} - (1-\mu)\boldsymbol{J}_e(\boldsymbol{\theta},\mathbf{q}_e)\dot{\mathbf{q}}_e \tag{6}$$

where μ is a real parameter. The true tip rates are captured by $\mu = 1$ while $\mu = 0$ considers only joint-induced motion. For $\mu = -1$, we obtain the multivariable analog of the reflected tip position. The variable $\boldsymbol{\rho}_\mu$ will be referred to as the *μ-tip position* and a technique for its determination will be discussed in Section V. Ultimately, we desire a control scheme which provides tracking of a prescribed trajectory by the true end-effector motions $\{\boldsymbol{\rho}, \dot{\boldsymbol{\rho}}\}$.

III. Approximate Dynamics for Large Payloads

Define the rigid mass matrices (relative to the body frame) of each link in the chain by

$$\boldsymbol{M}_{n,rr} \triangleq \begin{bmatrix} m_n\mathbf{1} & -\mathbf{c}_n^\times \\ \mathbf{c}_n^\times & \mathbf{J}_n \end{bmatrix}, \quad n = 1,\cdots,N+1 \tag{7}$$

where m_n, $\mathbf{c}_n$, and $\mathbf{J}_n$ are the mass, first, and second moments of inertia respectively defined with respect to F_n. The payload mass matrix is given the special designation $\boldsymbol{M}_t \equiv \boldsymbol{M}_{N+1,rr}$ and we assume that the payload is much more massive than the individual links, i.e., $\boldsymbol{M}_t \gg \boldsymbol{M}_{n,rr}$, $n = 1\cdots N$ (the ordering is the usual one for symmetric positive-definite matrices). It is also assumed that $N = 6$ (the corresponding rigid manipulator is nonredundant) and the manipulator trajectories are such that the rigid Jacobian matrix $\boldsymbol{J}_\theta$ is invertible.

The rest of this section is devoted to developing an appropriate form of (1) under the above assumptions. The kinetic energy for $\dot{\boldsymbol{\rho}} \neq \mathbf{0}$ can be approximated by that residing within the payload

$$T \doteq T_\rho \triangleq \tfrac{1}{2}\boldsymbol{v}_t^T\boldsymbol{M}_t\boldsymbol{v}_t = \tfrac{1}{2}\dot{\boldsymbol{\rho}}^T\boldsymbol{P}_t^T(\boldsymbol{\rho})\boldsymbol{M}_t\boldsymbol{P}_t(\boldsymbol{\rho})\dot{\boldsymbol{\rho}}. \tag{8}$$

This estimate can be refined by augmenting T_ρ with the kinetic energy consistent with $\dot{\boldsymbol{\rho}} \equiv \mathbf{0}$ which implies that $\dot{\boldsymbol{\theta}} = -\boldsymbol{J}_\theta^{-1}\boldsymbol{J}_e\dot{\mathbf{q}}_e$. Impressing this constraint on the kinetic energy, T in (2) becomes

$$T|_{\dot{\boldsymbol{\rho}}=0} = T_e \triangleq \tfrac{1}{2}\dot{\mathbf{q}}_e\widehat{\boldsymbol{M}}_{ee}(\mathbf{q})\dot{\mathbf{q}}_e, \quad \widehat{\boldsymbol{M}}_{ee}(\mathbf{q}) \triangleq \boldsymbol{B}_e^T(\mathbf{q})\boldsymbol{M}(\mathbf{q})\boldsymbol{B}_e(\mathbf{q}) \tag{9}$$

where $\boldsymbol{B}_e^T \triangleq [-\boldsymbol{J}_e^T\boldsymbol{J}_\theta^{-T} \quad \mathbf{1}]$. It is easy to show that $\widehat{\boldsymbol{M}}_{ee}$ formed in this fashion is independent of $\boldsymbol{M}_t$ since the contribution of (8) is effectively removed from T_e by the substitution for $\dot{\boldsymbol{\theta}}$. We propose that the total kinetic energy be approximated by

$$T \doteq T_\rho + T_e = \tfrac{1}{2}\boldsymbol{v}_t^T\boldsymbol{M}_t\boldsymbol{v}_t + \tfrac{1}{2}\dot{\mathbf{q}}_e^T\widehat{\boldsymbol{M}}_{ee}(\mathbf{q})\dot{\mathbf{q}}_e. \tag{10}$$

A more rigorous interpretation of (10) is possible. If $\boldsymbol{M}_t = \varepsilon_t^{-1}\widehat{\boldsymbol{M}}_t$ then the kinetic energy for small ε_t can be expanded as $T(\varepsilon_t) = T(0) + \mathcal{O}(\varepsilon_t)$. The energy T_e can be identified with $T(0)$ since for $\varepsilon_t = 0$ the payload becomes infinitely massive and the end-effector presents a clamped boundary condition to the manipulator. The expression T_ρ captures the additional contribution to the energy for a payload with large but finite mass properties (i.e., neglecting the links). The approach can also be justified on the basis of the results in [15]: the unconstrained modes of vibration corresponding to the setpoint linearization of (1) satisfy clamped boundary conditions at the end-effector owing to the large payload assumption.

The potential energy has been noted in (2) and in the sequel we shall apply Lagrange's equations with generalized coordinates $\{\boldsymbol{\rho}, \mathbf{q}_e\}$. From (3), the virtual displacements satisfy $\delta\boldsymbol{\rho} = \boldsymbol{J}_\theta\delta\boldsymbol{\theta} + \boldsymbol{J}_e\delta\mathbf{q}_e$ and the virtual work performed by the joint torques is

$$\delta W_e = \boldsymbol{\tau}^T\delta\boldsymbol{\theta} = \boldsymbol{\tau}^T\boldsymbol{J}_\theta^{-1}\delta\boldsymbol{\rho} - \boldsymbol{\tau}^T\boldsymbol{J}_\theta^{-1}\boldsymbol{J}_e\delta\mathbf{q}_e. \tag{11}$$

The system Lagrangian is $L = T_\rho + T_e - V$ and with a view to modeling structural damping, Rayleigh's dissipation function is taken to be $R = \frac{1}{2}\dot{\mathbf{q}}_e^T\boldsymbol{D}_{ee}\dot{\mathbf{q}}_e$. Realizing that T_e is formed with $\dot{\boldsymbol{\rho}} \equiv \mathbf{0}$, Lagrange's equations yield

$$\frac{d}{dt}\left(\frac{\partial T_\rho}{\partial\dot{\boldsymbol{\rho}}}\right) - \frac{\partial T_\rho}{\partial\boldsymbol{\rho}} = \boldsymbol{J}_\theta^{-T}\boldsymbol{\tau},$$
$$\frac{d}{dt}\left(\frac{\partial T_e}{\partial\dot{\mathbf{q}}_e}\right) + \frac{\partial R}{\partial\dot{\mathbf{q}}_e} - \frac{\partial L}{\partial\mathbf{q}_e} = -\boldsymbol{J}_e^T\boldsymbol{J}_\theta^{-T}\boldsymbol{\tau}. \tag{12}$$

The first of these coupled with the definition of T_ρ yields the dynamics of a free rigid body with generalized force distribution $\boldsymbol{J}_\theta^{-T}\boldsymbol{\tau}$. In [16], it is noted that these are equivalent to the quasi-Lagrangian body frame equations

$$\boldsymbol{M}_t\dot{\boldsymbol{v}}_t + \boldsymbol{v}_t^\otimes\boldsymbol{M}_t\boldsymbol{v}_t = \widehat{\boldsymbol{J}}_\theta^{-T}\boldsymbol{\tau}(t) \tag{13}$$

where the (generalized) force distribution has been expressed in F_{N+1}.

Expanding the elastic equation of (12) completes the desired form of the approximate dynamics:

$$\widehat{\boldsymbol{M}}_{ee}(\mathbf{q})\ddot{\mathbf{q}}_e + \boldsymbol{D}_{ee}\dot{\mathbf{q}}_e + \boldsymbol{K}_{ee}\mathbf{q}_e(t) = -\widehat{\boldsymbol{J}}_e^T\widehat{\boldsymbol{J}}_\theta^{-T}\boldsymbol{\tau}(t) + \boldsymbol{C}_e(\mathbf{q},\dot{\mathbf{q}}_e)\dot{\mathbf{q}}_e \tag{14}$$

where $\boldsymbol{C}_e(\mathbf{q},\dot{\mathbf{q}}_e)\dot{\mathbf{q}}_e = -\dot{\widehat{\boldsymbol{M}}}_{ee}\dot{\mathbf{q}}_e + \frac{1}{2}\partial T_e/\partial\mathbf{q}_e$. Since T_e is formed under the assumption that $\dot{\boldsymbol{\rho}} \equiv \mathbf{0}$, $\dot{\widehat{\boldsymbol{M}}}_{ee} = \sum_k \dot{q}_{ek}\partial\widehat{\boldsymbol{M}}_{ee}/\partial q_{ek}$ ($\boldsymbol{\rho}$ is not varied). Using the approach of [1] in the rigid robot case, it is readily shown that the matrix $\boldsymbol{C}_e$ can be chosen so that $2\boldsymbol{C}_e + \dot{\widehat{\boldsymbol{M}}}_{ee}$ is skew-symmetric. Equation (14) is a refinement of the result derived in [15], which ignored structural damping and the inertia forces associated with the link bodies, i.e., $\widehat{\boldsymbol{M}}_{ee} = \boldsymbol{D}_{ee} = \boldsymbol{C}_e \equiv \mathbf{O}$. These substitutions in (14) produce a *static* approximation for $\mathbf{q}_e$ which, in [15], predicted the elastic displacements quite accurately in a simulation context.

Now, consider the Hamiltonian $H_0 = T + V$ with T given by (10). Differentiating with respect to time and using (13) and (14) gives

$$\dot{H}_0 = \boldsymbol{v}_t^T\boldsymbol{M}_t\dot{\boldsymbol{v}}_t + \dot{\mathbf{q}}_e^T[\widehat{\boldsymbol{M}}_{ee}\ddot{\mathbf{q}}_e + \boldsymbol{K}_{ee}\mathbf{q}_e + \tfrac{1}{2}\dot{\widehat{\boldsymbol{M}}}_{ee}\dot{\mathbf{q}}_e] = \boldsymbol{\tau}^T\dot{\boldsymbol{\theta}} - \dot{\mathbf{q}}_e^T\boldsymbol{D}_{ee}\dot{\mathbf{q}}_e \tag{15}$$

where (4), the property of $\boldsymbol{v}_t^\otimes$ in (5), and the skew-symmetry of $2\boldsymbol{C}_e + \dot{\widehat{\boldsymbol{M}}}_{ee}$ have been duly noted. Hence, the energy balance of the exact system (1) is preserved by the approximate dynamics (13) and (14).

The system dynamics consistent with the constraint $\boldsymbol{v}_t = \boldsymbol{P}_t\dot{\boldsymbol{\rho}} = \mathbf{0}$ are the zero dynamics of the system with the end-effector rates as the output. For generic flexible manipulators, the zero dynamics are typically unstable [13] and the system is said to be nonminimum phase. For large payloads, $\boldsymbol{v}_t \equiv \mathbf{0}$ and (13) imply that $\boldsymbol{\tau} \equiv \mathbf{0}$ which when substituted into (14) yields the zero dynamics. Hence, in this limiting case, the zero dynamics are stable but unobservable from $\dot{\boldsymbol{\rho}}$ or $\boldsymbol{\rho}$ which is consistent with the clamped nature of the vibration modes already noted. This behavior is consistent with [13] where the transfer function from τ to an end-effector coordinate in the single link case was shown to be minimum phase as the mass of the link was shifted toward the endpoint. The lack of observability of $\dot{\mathbf{q}}_e$ from $\dot{\boldsymbol{\rho}}$ for large payloads is part of the motivation for introducing the μ-tip position and rate. In the next section, it will be shown that passivity is possible using $\dot{\boldsymbol{\rho}}_\mu$ as the output. This represents a stronger condition than the minimum phase property since passivity implies Lyapunov stability of the zero dynamics [17].

IV. Passivity Analysis and Feedforward Design

We now consider the input-output properties of the approximate dynamics. A recent account of the general theory is [18]; see also

[4]. The following notation will be used repeatedly:

$$\hat{\tau}(t) \triangleq \boldsymbol{J}_\theta^{-T}\tau(t). \tag{16}$$

(Omitted arguments of the Jacobian matrices imply quantities measured along the trajectory.) Equations (13), (14), and (6) are interpreted as an operator $\boldsymbol{G} : L_{2e} \rightarrow L_{2e}$ implementing the map $\dot{\boldsymbol{\rho}}_\mu = \boldsymbol{G}(\hat{\tau})$ (see [18] for a definition of the extended space L_{2e}). A system $\boldsymbol{H}$ with input $\mathbf{u} \in L_{2e}$ and output $\mathbf{y} = \boldsymbol{H}(\mathbf{u}) \in L_{2e}$ is *strictly passive* if there exists $\varepsilon > 0$ such that

$$\int_0^T \mathbf{u}^T \boldsymbol{H}(\mathbf{u})\, dt \geq \varepsilon \int_0^T \mathbf{u}^T\mathbf{u}\, dt, \quad \forall \mathbf{u} \in L_{2e},\ \forall T > 0. \tag{17}$$

If (17) is satisfied with $\varepsilon = 0$, then the system is *passive*. We now establish this property for $\boldsymbol{G}$.

Lemma 1: The map from $\hat{\tau}$ to $\dot{\boldsymbol{\rho}}_\mu$ is passive for $\mu < 1$.

Proof: Consider the nonnegative function

$$H_\mu = H_0 - \mu(T_e + V) = T_\rho + (1-\mu)(T_e + V), \quad \mu < 1$$

where T_ρ, T_e, and V are the kinetic and strain energies defined in (8), (9), and (2), respectively. Differentiating H_μ with respect to time and using (2) [or (15)] and (14) gives

$$\begin{aligned}\dot{H}_\mu &= \dot{H}_0 - \mu(\dot{T}_e + \dot{V}) \\ &= \tau^T\dot{\boldsymbol{\theta}} - \dot{\mathbf{q}}_e^T\boldsymbol{D}_{ee}\dot{\mathbf{q}}_e - \mu\dot{\mathbf{q}}_e^T(\widehat{\boldsymbol{M}}_{ee}\ddot{\mathbf{q}}_e + \boldsymbol{K}_{ee}\mathbf{q}_e + \tfrac{1}{2}\dot{\widehat{\boldsymbol{M}}}_{ee}\dot{\mathbf{q}}_e) \\ &= \hat{\tau}^T\boldsymbol{J}_\theta\dot{\boldsymbol{\theta}} + \mu\dot{\mathbf{q}}_e^T\boldsymbol{J}_e^T\boldsymbol{J}_\theta^{-T}\tau - (1-\mu)\dot{\mathbf{q}}_e^T\boldsymbol{D}_{ee}\dot{\mathbf{q}}_e \\ &= \hat{\tau}^T\dot{\boldsymbol{\rho}}_\mu - (1-\mu)\dot{\mathbf{q}}_e^T\boldsymbol{D}_{ee}\dot{\mathbf{q}}_e. \end{aligned} \tag{18}$$

Integrating the above relationship while taking $\mu < 1$ gives

$$\int_0^T \hat{\tau}^T\dot{\boldsymbol{\rho}}_\mu\, dt = H_\mu(T) - H_\mu(0) + (1-\mu) \cdot \int_0^T \dot{\mathbf{q}}_e^T\boldsymbol{D}_{ee}\dot{\mathbf{q}}_e\, dt \geq H_\mu(T) - H_\mu(0). \tag{19}$$

Consistent with an input-output treatment, we set $H_\mu(0) = 0$ which establishes the result. □

Setting $\hat{\tau} = \mathbf{0}$ in (18) shows that the function H_μ is a Lyapunov function for the unforced system. When $\mu = 0$, $\hat{\tau}^T\dot{\boldsymbol{\rho}}_\mu\big|_{\mu=0} = \tau^T\dot{\boldsymbol{\theta}}$ and Lemma 1 expresses the inherent passivity between the joint torques and joint rates.

We now establish a feedforward law which preserves the passivity property of Lemma 1 for the tracking error dynamics. Let $\{\boldsymbol{\rho}_d, \dot{\boldsymbol{\rho}}_d\}$ designate a prescribed Cartesian end-effector trajectory and define $\boldsymbol{v}_d \triangleq \boldsymbol{P}_t(\boldsymbol{\rho})\dot{\boldsymbol{\rho}}_d$. The tracking errors are defined by

$$\tilde{\boldsymbol{\rho}} \triangleq \boldsymbol{\rho} - \boldsymbol{\rho}_d, \quad \tilde{\boldsymbol{v}}_t \triangleq \boldsymbol{v}_t - \boldsymbol{v}_d = \boldsymbol{P}_t(\boldsymbol{\rho})\dot{\tilde{\boldsymbol{\rho}}}. \tag{20}$$

Guided by (13), express the joint torque as

$$\tau = \tau_d + \tilde{\tau}, \quad \tau_d \triangleq \widehat{\boldsymbol{J}}_\theta^T(\boldsymbol{\theta}, \mathbf{q}_e)\left[\boldsymbol{M}_t\dot{\boldsymbol{v}}_d + \boldsymbol{v}_d^{\otimes}\boldsymbol{M}_t\boldsymbol{v}_t\right], \quad \boldsymbol{v}_d = \boldsymbol{P}_t(\boldsymbol{\rho})\dot{\boldsymbol{\rho}}_d \tag{21}$$

where τ_d is the feedforward part and $\tilde{\tau}$ is interpreted as the feedback portion of the torque.

Define an estimate for the elastic displacements produced by the application of $\tau_d(t)$, $\mathbf{q}_{ed}(t)$, according to the solution of

$$\begin{aligned}&\widehat{\boldsymbol{M}}_{ee}(\mathbf{q})\ddot{\mathbf{q}}_{ed} + \boldsymbol{D}_{ee}\dot{\mathbf{q}}_{ed} + \boldsymbol{K}_{ee}\mathbf{q}_{ed} = \\ &\quad -\widehat{\boldsymbol{J}}_e^T\widehat{\boldsymbol{J}}_\theta^{-T}\tau_d + \boldsymbol{C}_e(\mathbf{q}, \dot{\mathbf{q}}_e)\dot{\mathbf{q}}_{ed}, \quad \mathbf{q}_{ed}(0) = \dot{\mathbf{q}}_{ed}(0) = \mathbf{0}. \end{aligned} \tag{22}$$

Notice that $\mathbf{q}_{ed}$ is not an arbitrary trajectory in the sense that $\boldsymbol{\rho}_d$ is; rather, it is determined by the feedforward τ_d which is determined by $\{\boldsymbol{\rho}_d(t), \dot{\boldsymbol{\rho}}_d(t)\}$. For this reason, $\mathbf{q}_{ed}$ is inherently reachable being defined as a solution of the motion equation in response to a given torque.

Substituting (21) into (13) and subtracting (22) from (14) gives the following description of the error dynamics:

$$\boldsymbol{M}_t\dot{\tilde{\boldsymbol{v}}}_t + \tilde{\boldsymbol{v}}_t^{\otimes}\boldsymbol{M}_t\boldsymbol{v}_t = \widehat{\boldsymbol{J}}_\theta^{-T}\tilde{\tau} \tag{23}$$

$$\begin{aligned}&\widehat{\boldsymbol{M}}_{ee}(\mathbf{q})\ddot{\tilde{\mathbf{q}}}_e + \boldsymbol{D}_{ee}\dot{\tilde{\mathbf{q}}}_e + \boldsymbol{K}_{ee}\tilde{\mathbf{q}}_e = \\ &\quad -\widehat{\boldsymbol{J}}_e^T\widehat{\boldsymbol{J}}_\theta^{-T}\tilde{\tau} + \boldsymbol{C}_e(\mathbf{q}, \dot{\mathbf{q}}_e)\dot{\tilde{\mathbf{q}}}_e, \quad \tilde{\mathbf{q}}_e = \mathbf{q}_e - \mathbf{q}_{ed}. \end{aligned} \tag{24}$$

The desired trajectory for $\boldsymbol{\rho}_\mu$, $\boldsymbol{\rho}_{\mu d}$, is defined by its time derivative using the last form in (6):

$$\dot{\boldsymbol{\rho}}_{\mu d} = \dot{\boldsymbol{\rho}}_d - (1-\mu)\boldsymbol{J}_e(\boldsymbol{\theta}, \mathbf{q}_e)\dot{\mathbf{q}}_{ed}. \tag{25}$$

Hence, using (6) and (25),

$$\dot{\tilde{\boldsymbol{\rho}}}_\mu = \dot{\tilde{\boldsymbol{\rho}}} - (1-\mu)\boldsymbol{J}_e\dot{\tilde{\mathbf{q}}}_e, \quad \tilde{\boldsymbol{\rho}}_\mu \triangleq \boldsymbol{\rho}_\mu - \boldsymbol{\rho}_{\mu d}. \tag{26}$$

It will be important to realize that $\tilde{\boldsymbol{\rho}}_\mu \equiv \mathbf{0}$ and $\tilde{\mathbf{q}}_e \equiv \mathbf{0}$ imply that $\tilde{\boldsymbol{\rho}} \equiv \mathbf{0}$. We now establish the passivity of the tracking error dynamics.

Theorem 1: The mapping $\dot{\tilde{\boldsymbol{\rho}}}_\mu = \boldsymbol{G}(\boldsymbol{J}_\theta^{-T}\tilde{\tau})$, where $\boldsymbol{G}$ is determined by (23)–(26), is passive for $\mu < 1$.

Proof: Define the nonnegative function

$$\mathcal{S}_\mu = \tfrac{1}{2}\tilde{\boldsymbol{v}}_t^T\boldsymbol{M}_t\tilde{\boldsymbol{v}}_t + \tfrac{1}{2}(1-\mu)[\dot{\tilde{\mathbf{q}}}_e^T\widehat{\boldsymbol{M}}_{ee}\dot{\tilde{\mathbf{q}}}_e + \tilde{\mathbf{q}}_e^T\boldsymbol{K}_{ee}\tilde{\mathbf{q}}_e], \quad \mu < 1.$$

Differentiating the above with respect to time and using (23) and (24) gives

$$\begin{aligned}\dot{\mathcal{S}}_\mu &= \tilde{\boldsymbol{v}}_t^T\boldsymbol{M}_t\dot{\tilde{\boldsymbol{v}}}_t + (1-\mu)\dot{\tilde{\mathbf{q}}}_e^T[\widehat{\boldsymbol{M}}_{ee}(\mathbf{q})\ddot{\tilde{\mathbf{q}}}_e + \boldsymbol{K}_{ee}\tilde{\mathbf{q}}_e + \tfrac{1}{2}\dot{\widehat{\boldsymbol{M}}}_{ee}\dot{\tilde{\mathbf{q}}}_e] \\ &= \tilde{\boldsymbol{v}}_t^T[-\tilde{\boldsymbol{v}}_t^{\otimes}\boldsymbol{M}_t\boldsymbol{v}_t + \widehat{\boldsymbol{J}}_\theta^{-T}\tilde{\tau}] - (1-\mu)\dot{\tilde{\mathbf{q}}}_e^T[\widehat{\boldsymbol{J}}_e^T\widehat{\boldsymbol{J}}_\theta^{-T}\tilde{\tau} + \boldsymbol{D}_{ee}\dot{\tilde{\mathbf{q}}}_e] \\ &= \left[\tilde{\boldsymbol{v}}_t - (1-\mu)\widehat{\boldsymbol{J}}_e\dot{\tilde{\mathbf{q}}}_e\right]^T\widehat{\boldsymbol{J}}_\theta^{-T}\tilde{\tau} - (1-\mu)\dot{\tilde{\mathbf{q}}}_e^T\boldsymbol{D}_{ee}\dot{\tilde{\mathbf{q}}}_e \\ &= \dot{\tilde{\boldsymbol{\rho}}}_\mu^T(\boldsymbol{J}_\theta^{-T}\tilde{\tau}) - (1-\mu)\dot{\tilde{\mathbf{q}}}_e^T\boldsymbol{D}_{ee}\dot{\tilde{\mathbf{q}}}_e. \end{aligned} \tag{27}$$

Integrating the above relationship gives

$$\int_0^T \dot{\tilde{\boldsymbol{\rho}}}_\mu^T(\boldsymbol{J}_\theta^{-T}\tilde{\tau})\, dt = \mathcal{S}_\mu(T) - \mathcal{S}_\mu(0) + (1-\mu) \cdot \int_0^T \dot{\tilde{\mathbf{q}}}_e^T\boldsymbol{D}_{ee}\dot{\tilde{\mathbf{q}}}_e dt \geq \mathcal{S}_\mu(T) - \mathcal{S}_\mu(0) \tag{28}$$

which establishes the result upon setting $\mathcal{S}_\mu(0) = 0$. □

V. Feedback Design and Lyapunov Stability Analysis

With reference to the feedback system in Fig. 1, the passivity theorem states that if $\boldsymbol{G} : L_{2e} \rightarrow L_{2e}$ is passive and $\boldsymbol{H} : L_{2e} \rightarrow L_{2e}$ is strictly passive then the feedback system depicted in Fig. 1 is L_2-stable, i.e., if $\mathbf{u} \in L_2$ (a bounded disturbance torque) then $\dot{\tilde{\boldsymbol{\rho}}}_\mu \in L_2$. Based on the passivity theorem, we select the feedback portion of the controller to be

$$\tilde{\tau} = -\boldsymbol{J}_\theta^T(\boldsymbol{\theta}, \mathbf{q}_e)\boldsymbol{H}(\dot{\tilde{\boldsymbol{\rho}}}_\mu), \quad \boldsymbol{H}(\cdot) = \mathbf{K}_d(\cdot) + \mathbf{K}_p\int_0^t (\cdot)\, d\tau \tag{29}$$

where $\mathbf{K}_d = \mathbf{K}_d^T > 0$ and $\mathbf{K}_p = \mathbf{K}_p^T > 0$. Although $\boldsymbol{H}(\cdot)$ can be any strictly passive operator, we have selected a PI law (a PD law with respect to $\tilde{\boldsymbol{\rho}}_\mu$) to keep the presentation simple. Since the integral operator is passive (see [4]) and a positive gain is strictly passive, $\boldsymbol{H}$ is also strictly passive. The main advantage of the input-output approach is the specification of a large family of stabilizing controllers. However, there is no analog of the LaSalle invariance principle which is ultimately needed to show that the position errors are well-behaved. Hence, a Lyapunov approach is employed below using the Lyapunov function suggested by Theorem 1.

Theorem 2: The equilibrium $\tilde{\boldsymbol{\rho}} = \dot{\tilde{\boldsymbol{\rho}}} = \tilde{\mathbf{q}}_e = \dot{\tilde{\mathbf{q}}}_e \equiv \mathbf{0}$ of the closed-loop system given by (23)–(26) and (29) is globally asymptotically stable if $\mu < 1$.

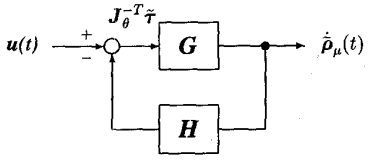

Fig. 1. Feedback system.

Proof: We adopt as a Lyapunov function

$$\mathcal{V} = \mathcal{S}_\mu + \tfrac{1}{2}\tilde{\boldsymbol{\rho}}_\mu^T \mathbf{K}_p \tilde{\boldsymbol{\rho}}_\mu, \quad \mu < 1 \tag{30}$$

which is easily shown to be positive-definite in the state $\mathbf{x} \triangleq \text{col}\{\dot{\tilde{\boldsymbol{\rho}}}, \dot{\tilde{\mathbf{q}}}_e, \tilde{\boldsymbol{\rho}}, \tilde{\mathbf{q}}_e\}$. Using (27) and (29), we have

$$\begin{aligned}\dot{\mathcal{V}} &= \dot{\mathcal{S}}_\mu + \dot{\tilde{\boldsymbol{\rho}}}_\mu^T \mathbf{K}_p \tilde{\boldsymbol{\rho}}_\mu \\ &= \dot{\tilde{\boldsymbol{\rho}}}_\mu^T \left[\boldsymbol{J}_\theta^{-T} \tilde{\boldsymbol{\tau}} + \mathbf{K}_p \tilde{\boldsymbol{\rho}}_\mu \right] - (1-\mu) \dot{\tilde{\mathbf{q}}}_e^T \boldsymbol{D}_{ee} \dot{\tilde{\mathbf{q}}}_e \\ &= -\dot{\tilde{\boldsymbol{\rho}}}_\mu^T \mathbf{K}_d \dot{\tilde{\boldsymbol{\rho}}}_\mu - (1-\mu) \dot{\tilde{\mathbf{q}}}_e^T \boldsymbol{D}_{ee} \dot{\tilde{\mathbf{q}}}_e. \end{aligned} \tag{31}$$

The original form of LaSalle's Theorem only applied to autonomous systems; the system here is nonautonomous owing to the configuration dependence on $\boldsymbol{\rho}_d(t)$ and $\dot{\boldsymbol{\rho}}_d(t)$. However, the invariance principle extends to nonautonomous systems which exhibit bounded dependence on t or are asymptotically autonomous [19]. Such is the case here if $\boldsymbol{\rho}_d(t) \to \bar{\boldsymbol{\rho}}_d$ (a constant) as $t \to \infty$. If $\dot{\mathcal{V}} \leq -W(\mathbf{x})$ where $W(\mathbf{x}) \geq 0$, then all bounded solutions tend to the largest invariant set which satisfies $W(\mathbf{x}) \equiv 0$. From (30) and (31), all solutions are bounded. Using the invariance principle and setting $\dot{\tilde{\boldsymbol{\rho}}}_\mu = \dot{\tilde{\mathbf{q}}}_e \equiv \mathbf{0}$, it follows from (26) and (20) that $\tilde{\boldsymbol{\rho}} = \tilde{\boldsymbol{v}}_t \equiv \mathbf{0}$. From (23), $\tilde{\boldsymbol{\tau}} \equiv \mathbf{0}$ and then (24) shows that $\tilde{\mathbf{q}}_e \equiv \mathbf{0}$. The control law (29) then gives $\tilde{\boldsymbol{\rho}}_\mu \equiv \mathbf{0}$ and we conclude that $\tilde{\boldsymbol{\rho}} \to \mathbf{0}$. □

Although any strictly passive feedback controller can be used, linear time-invariant ones are desirable from an implementation standpoint. Included in this class are some strictly positive real transfer functions. Even simpler is the PD law used here. The design is most easily carried out for a linearization of the system but we are guaranteed that it will stabilize the nonlinear passive system. Substituting (29) into (21) gives the combined feedforward/feedback controller

$$\boldsymbol{\tau}(t) = \widehat{\boldsymbol{J}}_\theta^T(\boldsymbol{\theta}, \mathbf{q}_e) \left[\boldsymbol{M}_t \dot{\boldsymbol{v}}_d + \boldsymbol{v}_d^{\otimes} \boldsymbol{M}_t \boldsymbol{v}_t \right] - \boldsymbol{J}_\theta^T(\boldsymbol{\theta}, \mathbf{q}_e) \left[\mathbf{K}_d \dot{\tilde{\boldsymbol{\rho}}}_\mu + \mathbf{K}_p \tilde{\boldsymbol{\rho}}_\mu \right]. \tag{32}$$

Let us linearize the system (1) in the vicinity of a constant target $\boldsymbol{\rho}_d = \bar{\boldsymbol{\rho}}$ ($\mathbf{q}_e = \mathbf{0}$) with corresponding joint angles $\bar{\boldsymbol{\theta}}$. The target configuration vector is $\bar{\mathbf{q}} = \text{col}\{\bar{\boldsymbol{\theta}}, \mathbf{0}\}$ and let $\delta\mathbf{q} = \mathbf{q} - \bar{\mathbf{q}}$, $\delta\boldsymbol{\rho}_\mu = \boldsymbol{\rho}_\mu - \bar{\boldsymbol{\rho}}$. The linearized forms of the the kinematics (6) and the dynamics (1) with $\boldsymbol{D}_{ee} = \mathbf{O}$ can be written as

$$\delta\boldsymbol{\rho}_\mu = \bar{\boldsymbol{J}}_\theta \delta\boldsymbol{\theta} + \mu \bar{\boldsymbol{J}}_e \mathbf{q}_e, \quad \bar{\boldsymbol{M}} \delta\ddot{\mathbf{q}} + \boldsymbol{K} \delta\mathbf{q} = \boldsymbol{B}\boldsymbol{\tau}. \tag{33}$$

The overbar notation $\bar{(\cdot)}$ designates configuration dependent quantities evaluated at the setpoint $\bar{\boldsymbol{\theta}}$. It was shown in [15] that the transfer matrix relating $\bar{\boldsymbol{J}}_\theta^{-T}\boldsymbol{\tau}$ to $\delta\dot{\boldsymbol{\rho}}_\mu$ was positive real under the payload assumption made here. Furthermore, the vibrational modes were shown to be unobservable from $\delta\boldsymbol{\rho}_\mu$ or $\delta\dot{\boldsymbol{\rho}}_\mu$ when $\mu = 1$. A valuable use for $\mu < 1$ is the introduction of the vibrational modes into controller input. Indeed, this is essential since they will typically be lightly damped.

Equation (33) along with the the linearized form of the control law (29) ($\dot{\boldsymbol{v}}_d = \mathbf{0}$) will be used for analysis of the controller gains. An obvious choice for $\mathbf{K}_p$ and $\mathbf{K}_d$ is

$$\mathbf{K}_p = \Omega^2 \bar{\boldsymbol{P}}_t^T \boldsymbol{M}_t \bar{\boldsymbol{P}}_t, \quad \mathbf{K}_d = 2\zeta\Omega \bar{\boldsymbol{P}}_t^T \boldsymbol{M}_t \bar{\boldsymbol{P}}_t \tag{34}$$

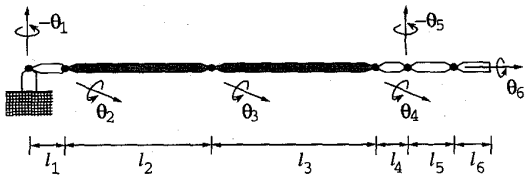

Fig. 2. Architecture of the SRMS.

TABLE I
PROPERTIES OF THE SRMS

Property	ℓ (m)	Mass (kg)	J_n^r (kg·m²)	J_n^p (kg·m²)	J_n^y (kg·m²)
Link 1	0.9	95.0	0.2	25.75	25.75
Link 2	6.4	138.0	0.4	1884.36	1884.36
Link 3	7.0	85.0	0.4	1388.53	1388.53
Link 4	0.5	8.0	0.2	0.76	0.76
Link 5	0.8	44.0	0.2	9.49	9.49
Link 6	0.6	41.0	0.2	5.02	5.02
Payload	–	15,000	30,000	515,000	515,000
Elastic Stiffnesses	EI (N·m²)		GJ (N·m²)		EA (N)
Link 2	4.046×10^6		2.040×10^6		2.790×10^9
Link 3	2.812×10^6		1.417×10^6		1.194×10^9

which yields identical eigenvalues for the corresponding payload-dominated rigid system.

It would be desirable if $\dot{\boldsymbol{\rho}}_\mu$ and $\boldsymbol{\rho}_\mu$ could be constructed from joint measurements $\{\boldsymbol{\theta}(t), \dot{\boldsymbol{\theta}}(t)\}$ and tip measurements $\{\boldsymbol{\rho}(t), \dot{\boldsymbol{\rho}}(t)\}$ alone, which would excuse the requirement for direct measurement of the elastic coordinates $\mathbf{q}_e$. However, the latter are required in the evaluation of the Jacobian matrix $\boldsymbol{J}_\theta(\boldsymbol{\theta}, \mathbf{q}_e)$ and the formation of the μ-tip positions and rates. Both problems can be avoided by approximating the Jacobian in (32) by $\boldsymbol{J}_\theta(\boldsymbol{\theta}, \mathbf{0})$ ($\widehat{\boldsymbol{J}}_\theta(\boldsymbol{\theta}, \mathbf{0})$ in the feedforward part). Furthermore, the penultimate form in (6) gives

$$\dot{\tilde{\boldsymbol{\rho}}}_\mu = \dot{\boldsymbol{\rho}}_\mu - \dot{\boldsymbol{\rho}}_{\mu d} \doteq \left[\mu\dot{\boldsymbol{\rho}} + (1-\mu)\boldsymbol{J}_\theta(\boldsymbol{\theta}, \mathbf{0})\dot{\boldsymbol{\theta}} \right] - \dot{\boldsymbol{\rho}}_d \tag{35}$$

where we have also set $\dot{\boldsymbol{\rho}}_{\mu d} \doteq \dot{\boldsymbol{\rho}}_d$ (hence $\boldsymbol{\rho}_{\mu d} \doteq \boldsymbol{\rho}_d$). This rids us of the need to construct $\mathbf{q}_{ed}$ and $\dot{\mathbf{q}}_{ed}$ and is justified on the grounds that our numerical results indicate that an appropriate value for μ is nearly 1. The μ-tip position error can be determined from the integral of (35):

$$\tilde{\boldsymbol{\rho}}_\mu = [\mu\boldsymbol{\rho}(t) + (1-\mu)\boldsymbol{F}(\boldsymbol{\theta})] - \boldsymbol{\rho}_d(t) \tag{36}$$

where $\boldsymbol{F}(\boldsymbol{\theta})$ represents the rigid forward kinematics map. A further simplification is possible if we take $\boldsymbol{v}_d = \boldsymbol{P}_t(\boldsymbol{\rho}_d)\dot{\boldsymbol{\rho}}_d$, i.e., replace $\boldsymbol{P}_t(\boldsymbol{\rho})$ with $\boldsymbol{P}_t(\boldsymbol{\rho}_d)$ in calculating $\boldsymbol{v}_d$ and $\dot{\boldsymbol{v}}_d$. In our numerical example, we shall incorporate the above simplifications into the controller (32).

VI. Numerical Example

The previous analytical results have been predicated on the veracity of the approximate motion equations. The goal of this section is to illustrate their validity and implement the proposed controllers using a simulation based on the full motion equations. The manipulator consists of six joints and is modeled after the Space Shuttle Remote Manipulator (SRMS) Arm. Included in the model is a payload, modeled by a cylindrical drum, which represents a spin-stabilized satellite, and the Space Shuttle (cantilevered for this example). The geometric and mass properties of the of the system are summarized

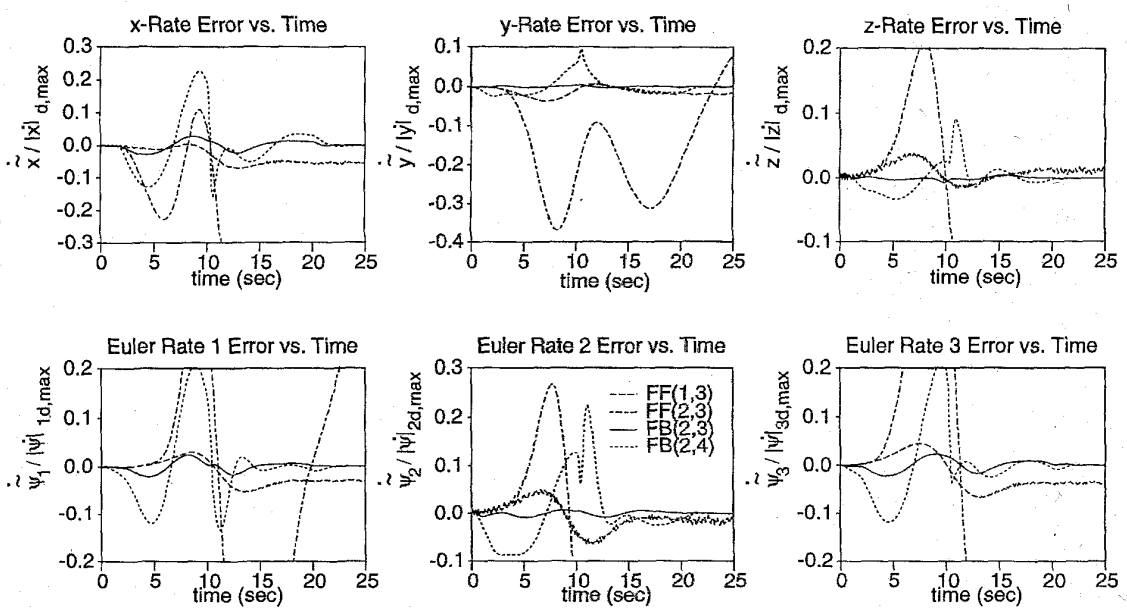

Fig. 3. End-effector velocity tracking errors (1 = full Jacobian, 2 = approximate Jacobian, 3 = known payload, and 4 = uncertain payload).

TABLE II
TRACKING ERRORS

controller	β_t	$E_{t\rho}$	$E_{b\rho}$	$E_{t\dot{\rho}}$	$E_{b\dot{\rho}}$	$\|\boldsymbol{\tau}_T\|_2$ (kN · m)
FF(1,3)	1.0	1.4×10^{-2}	1.9×10^{-2}	4.3×10^{-2}	5.9×10^{-2}	355.7
FF(2,3)	1.0	1.7×10^{-1}	2.8×10^{-1}	6.5×10^{-1}	7.8×10^{-1}	337.8
FB(2,3)	1.0	1.9×10^{-3}	5.1×10^{-3}	1.4×10^{-2}	2.0×10^{-2}	360.6
FB(2,4)	1.0	8.5×10^{-3}	2.9×10^{-2}	8.5×10^{-2}	1.3×10^{-1}	383.2
FB(2,3)	0.1	1.0×10^{-3}	3.1×10^{-3}	1.2×10^{-2}	1.7×10^{-2}	36.9
FB(2,3)	0.01	7.3×10^{-3}	1.8×10^{-2}	4.9×10^{-2}	5.9×10^{-2}	4.8
FB(2,3)	0.001	4.1×10^{-2}	7.8×10^{-2}	2.1×10^{-1}	1.8×10^{-1}	1.9

(1 = full jacobian, 2 = approx. jacobian, 3 = known payload, 4 = uncertain payload)

in Table I and the architecture of the Arm is shown in Fig. 2. The only flexible bodies are links 2 and 3 which are the lower and upper arm booms.

Each of the flexible booms is modeled using engineering beam theory and the exact cantilevered eigenfunctions are used for discretization. Each boom is modeled with six modes: two bending modes in each of the in-plane and out-of-plane directions, one stretch mode, and one torsional mode. The simulation model used here is the EEE model fully described in [20] (see also [21]). Structural damping is neglected in the simulation and the desired end-effector trajectory is generated as follows. The initial configuration corresponds to $\theta_n(0) = 0, n = 1 \cdots 6$, and the desired terminal configuration is $\theta_n(T) = 0.4$ rad, $n = 1 \cdots 6$, where $T = 20$ s. The prescribed trajectory $\{\boldsymbol{\rho}_d(t), \dot{\boldsymbol{\rho}}_d(t)\}$ is fashioned from the rigid forward kinematic solution corresponding to the joint trajectories

$$\theta_n(t) = (\theta_{nT} - \theta_{n0})\left(\frac{t}{T} - \frac{1}{2\pi}\sin\frac{2\pi t}{T}\right) + \theta_{n0}, \quad n = 1, \cdots, 6. \tag{37}$$

A 3-2-1 Euler sequence $\{\psi_1, \psi_2, \psi_3\}$ is used to characterize the end-effector orientation. We begin by analyzing the simulation values for $\tilde{\boldsymbol{\rho}} = \dot{\boldsymbol{\rho}} - \dot{\boldsymbol{\rho}}_d$, $\boldsymbol{\rho}(t) = [x \;\; y \;\; z \;\; \psi_1 \;\; \psi_2 \;\; \psi_3]^T$, in response to the feedforward portion of (32). The velocity tracking errors are given in Fig. 3 and have been normalized using the maximum absolute values of $\dot{\boldsymbol{\rho}}_d$. The Jacobian matrix for the curves labeled FF(1,3) have been calculated using the "measured" values of $\boldsymbol{\theta}(t)$ and $\mathbf{q}_e(t)$ obtained from the simulation. They show reasonable agreement between $\boldsymbol{\rho}$ and $\boldsymbol{\rho}_d$, thus demonstrating the validity of the approximate dynamics upon which the feedforward controller is based. If the elastic dependence in the rigid Jacobian matrix is suppressed, the curves labeled FF(2,3) are obtained. The tracking degradation illustrates the importance of the elastic coordinates in the Jacobian for the approximate dynamics solution.

As indicators of tracking performance, the following measures are adopted:

$$E_{t\rho} = \frac{\|\tilde{\boldsymbol{\rho}}_T\|_{2t}}{\|\boldsymbol{\rho}_{dT}\|_{2t}}, \quad E_{b\rho} = \frac{\|\tilde{\boldsymbol{\rho}}_T\|_{2b}}{\|\boldsymbol{\rho}_{dT}\|_{2b}},$$
$$E_{t\dot{\rho}} = \frac{\|\dot{\tilde{\boldsymbol{\rho}}}_T\|_{2t}}{\|\dot{\boldsymbol{\rho}}_{dT}\|_{2t}}, \quad E_{b\dot{\rho}} = \frac{\|\dot{\tilde{\boldsymbol{\rho}}}_T\|_{2b}}{\|\dot{\boldsymbol{\rho}}_{dT}\|_{2b}} \tag{38}$$

where T denotes truncation at $T = 20$ s, and the subscripts $2t$ and $2b$ refer to L_2-norms applied to the top (translational) and bottom (rotational) three-tuples of the argument, respectively. The tracking errors and the L_2-norm of the truncated torques will be gathered in Table II.

The validity of the elastic motion equation (14) can be established by comparing the natural frequencies of the system

$$\widehat{\boldsymbol{M}}_{ee}(\bar{\mathbf{q}})\ddot{\mathbf{q}}_e + \boldsymbol{K}_{ee}\mathbf{q}_e = \mathbf{0} \tag{39}$$

TABLE III
EIGENVALUES OF THE LINEARIZED SYSTEM

open-loop (rad/s)		closed-loop (rad/s)		
exact	approx.	$\mu = 1$	$\mu = 0.99$	$\mu = 0$
0, 0	—	$-1.78 \pm \jmath 0.60$	$-1.80 \pm \jmath 0.60$	$-1.84 \pm \jmath 0.57$
0, 0	—	$-1.88 \pm \jmath 0.44$	$-1.93 \pm \jmath 0.39$	$-1.70,\ -3.90$
0, 0	—	$-1.94 \pm \jmath 0.30$	$-1.99 \pm \jmath 0.20$	$-0.86 \pm \jmath 2.28$
0, 0	—	$-1.99 \pm \jmath 0.02$	$-2.19,\ -1.86$	$-0.38 \pm \jmath 1.75$
0, 0	—	$-1.99 \pm \jmath 0.01$	$-1.15 \pm \jmath 2.51$	$-0.01 \pm \jmath 0.33$
0, 0	—	$-2.07,\ -1.94$	$-0.97 \pm \jmath 2.41$	$-0.001 \pm \jmath 0.30$
$\pm\jmath 16.95$	$\pm\jmath 17.09$	$3.06 \pm \jmath 17.27$	$-1.43,\ -3203$	$-1.20, -376000$
$\pm\jmath 82.79$	$\pm\jmath 82.91$	$-2.39 \pm \jmath 82.96$	$-1.41, -37640$	$-1.21, -33800$
$\pm\jmath 97.69$	$\pm\jmath 98.37$	$3.27 \pm \jmath 98.15$	$-12.1 \pm \jmath 51.9$	$-1.31, -80895$
$\pm\jmath 100.9$	$\pm\jmath 102.4$	$4.31 \pm \jmath 102.7$	$-18.6 \pm \jmath 91.9$	$-1.41,\ -45749$
$\pm\jmath 198.5$	$\pm\jmath 198.7$	$1.83 \pm \jmath 198.7$	$-12.7 \pm \jmath 102.$	$-6.47, -1289$
$\pm\jmath 234.9$	$\pm\jmath 237.4$	$1.88 \pm \jmath 237.3$	$-14.4 \pm \jmath 227.$	$-2.32 \pm \jmath 74.3$
$\pm\jmath 385.4$	$\pm\jmath 385.5$	$-1.66 \pm \jmath 385.5$	$-167. \pm \jmath 148.$	$-5.98 \pm \jmath 184.$
$\pm\jmath 662.4$	$\pm\jmath 662.5$	$-9.28 \pm \jmath 662.8$	$-36.2 \pm \jmath 309.$	$-14.3 \pm \jmath 223.$
$\pm\jmath 706.2$	$\pm\jmath 706.9$	$-3.47 \pm \jmath 706.7$	$-104. \pm \jmath 629.$	$-208. \pm \jmath 220.$
$\pm\jmath 1057.$	$\pm\jmath 1059.$	$1.88 \pm \jmath 1059.$	$-41.6 \pm \jmath 1047$	$-17.9 \pm \jmath 711.$
$\pm\jmath 1399.$	$\pm\jmath 1402.$	$1.11 \pm \jmath 1402.$	$-288. \pm \jmath 1130$	$-60.7 \pm \jmath 910.$
$\pm\jmath 2996.$	$\pm\jmath 2998.$	$0.57 \pm \jmath 2998.$	$-39.1 \pm \jmath 2959$	$-2.52 \pm \jmath 2898$

with those of the undamped, unforced, linearized form of (1). The latter includes the six zero frequencies which are effectively removed from (39) by clamping the tip. The natural frequencies in both cases for the terminal configuration ($\theta_n \equiv 0.4$ rad) are given in Table III. The agreement is very good (within 1.6% for all modes) and showed steady improvement as the the payload mass and inertia were made larger (the frequencies were within 0.15% for a payload ten times more massive: $\boldsymbol{M}_t \rightarrow 10\boldsymbol{M}_t$).

The proposed feedback compensator is now added to the controller with $\mathbf{K}_p$ and $\mathbf{K}_d$ selected using (34) with $\Omega = 2$ rad/s and $\zeta = 1$. The eigenvalues of the closed-loop system given by (33) (terminal configuration) and (32) ($\boldsymbol{v}_d = \mathbf{0}$) are given in Table III for various values of μ. For $\mu = 1$, the system is slightly unstable but as the payload was made more massive (for fixed $\mathbf{K}_p$ and $\mathbf{K}_d$), the vibration modes migrated to the imaginary axis, tending toward complete unobservability. A value of $\mu = 0$, corresponding to joint and joint rate feedback, produces poor damping of some vibration modes and very overdamped response for the rigid modes. This was typical of small positive values and all negative values of μ.

As can be gleaned from the table, a value of $\mu = 0.99$ yields a good compromise between vibration damping and attainment of the target rigid eigenvalues. The velocity tracking errors using the controller specified by (32) with $\mu = 0.99$ are also given in Fig. 3 (curve FB(2,3)). All simplifications discussed in the last paragraph of Section V have been incorporated. The tracking performance is excellent despite the poor results observed when the feedforward component, without elastic information, was used alone. The situation where the control system designer's knowledge of $\boldsymbol{M}_t$ is replaced with $0.5\boldsymbol{M}_t$ for design of both the feedforward and feedback controllers is also illustrated in Fig. 3 (curve FB(2,4)). Stability is preserved and the tracking is still quite good in spite of badly-placed eigenvalues and a feedforward component which performs very poorly if used alone. The position graphs for both feedback controllers (not shown on account of space limitations) showed very little discernible difference between the simulated and prescribed end-effector trajectories.

For the previous simulation results, $m_7 = 36.5\left(\sum_{n=1}^{6} m_n\right)$. We now consider the situation where the true payload mass matrix $\boldsymbol{M}_t$ is replaced with $\beta_t \boldsymbol{M}_t$ ($\beta_t < 1$) and β_t is reduced in all facets: simulation model, feedforward design, and feedback gain selection. The closed-loop tracking errors also appear in Table II. The performance for $\beta_t = 0.1$ actually exceeds the baseline but smaller values lead to decline; instability was not observed. It should be borne in mind, that little attempt has been made to optimize the gains of the feedback controller. All trajectories shown here started in a kinematic singularity ($\boldsymbol{J}_\theta(\mathbf{0}, \mathbf{0})$ is singular) but this does not seem to have hindered performance.

VII. CONCLUDING REMARKS

The forward dynamics map from joint torques to tip rates is non-minimum phase (hence not passive) for a typical flexible manipulator. This paper has shown that when a large payload is involved, this map becomes rigid in character since the dynamics governing the elastic coordinates become unobservable from the tip. By introducing the μ-tip rates, the elastic coordinates were rendered observable and the map from torques (actually $\boldsymbol{J}_\theta^{-T}\boldsymbol{\tau}$) to μ-tip rates was shown to be passive. Using the rigid dynamics of the payload, we were able to create a feedforward torque which preserved passivity for the μ-tip rate tracking errors. Hence, stable tracking could then be demonstrated using a strictly passive feedback (a PD law in this case). This represents a significant extension of the single link case, which is SISO and linear, time-invariant, but at the expense of a large payload assumption.

The controllers presented here have a simple structure and represent a modest departure from those previously advocated for rigid manipulators. Although they require measurements of end-effector position and velocity in addition to the joint angles and rates, the elastic coordinates were not required for implementation. The presented simulation study demonstrated excellent tracking performance for the controller under the key assumption. Relaxation of the large payload assumption still led to reasonable controller performance. In this

light, it is possible that the success of the μ-tip rate concept can be explained with concepts other than passivity.

Although the base body, $\mathcal{B}_0$, has been constrained in this paper, this was largely to simplify the presentation. If it is replaced with a free, fully-actuated rigid spacecraft, then the passivity analysis is easily extended by augmenting the input vector to include the spacecraft actuation and augmenting the μ-tip rate with the spacecraft rates. There are many other important extensions. The simple PD feedback controller used here can be replaced with dynamic SPR compensation (plus a proportional term) whose systematic design for stabilization of nonlinear passive systems has been largely unexplored. We also note that the feedforward controller used here is linear in the payload mass properties. This characteristic coupled with the passive structure of the error dynamics permits the development of an adaptive version of the controller using techniques similar to those of the rigid case [1], [2].

References

[1] R. Ortega and M. W. Spong, "Adaptive motion control of rigid robots: A tutorial," *Automatica*, vol. 25, pp. 877–888, 1989.

[2] I. Landau and R. Horowitz, "Applications of the passive systems approach to the stability analysis of adaptive controllers for robot manipulators," *Int. J. Adaptive Contr. Signal Processing*, vol. 3, pp. 228, 1989.

[3] R. J. Benhabib, R. P. Iwens, and R. L. Jackson, "Stability of large space structure control systems using positivity concepts," *AIAA J. Guidance Contr.*, vol. 4, no. 5, pp. 487–494, Sept.-Oct. 1981.

[4] C. A. Desoer and M. Vidyasagar, *Feedback Systems: Input-Output Properties*. New York: Academic, 1975.

[5] J. C. Willems, "Dissipative dynamical systems, Part I: General theory; Part II: Linear systems with quadratic supply rates," *Arch. Rational Mech. Anal.*, vol. 45, pp. 321–393, 1972.

[6] D. J. Hill and P. J. Moylan, "Stability results for nonlinear feedback systems," *Automatica*, vol. 13, pp. 377–382, 1977.

[7] A. De Luca and B. Siciliano, "Inversion-based nonlinear control of robot arms with flexible links," *AIAA J. Guidance, Contr. Dyn.*, vol. 16, no. 6, pp. 1169–1176, Nov.-Dec. 1993.

[8] E. Bayo, M. A. Serna, P. Papadopoulus, and J. Stubbe, "Inverse dynamics and kinematics of multi-link elastic robots: An iterative frequency domain approach," *Int. J. Rob. Res.*, vol. 8, no. 6, pp. 49–62, 1989.

[9] D. Wang and M. Vidyasagar, "Passive control of a single flexible link," in *Proc. 1990 IEEE Int. Conf. Robotics and Automation*, Cincinnati, OH, May 1990, pp. 1432–1437.

[10] ——, "Transfer functions for a single flexible link," *Int. J. Robot. Res.*, vol. 10, no. 5, pp. 540–549, 1991.

[11] H. R. Pota and M. Vidyasagar, "Passivity of flexible beam transfer functions with modified outputs," in *Proc. 1991 IEEE Int. Conf. Robotics and Automation*, Sacramento, CA, Apr. 1991, pp. 2826–2831.

[12] E. Barbieri, "Single-input/single-output transfer functions for a flexible slewing link," *J. Robot. Syst.*, vol. 10, no. 7, pp. 913–929, 1993.

[13] A. De Luca, P. Lucibello, and G. Ulivi, "Inversion techniques for trajectory control of flexible robot arms," *J. Robot. Syst.*, vol. 6, no. 4, pp. 325–344, 1989.

[14] V. Feliu, K. S. Rattan, and H. B. Brown Jr., "Modeling and control of single-link flexible arms with lumped masses," *ASME J. Dyn. Syst., Meas., Contr.*, vol. 114, pp. 59–69, Mar. 1992.

[15] C. J. Damaren, "Passivity analysis for flexible multilink space manipulators," *AIAA J. Guidance, Contr., Dyn.*, vol. 18, no. 2, pp. 272–279, Mar.–Apr. 1995.

[16] P. C. Hughes, *Spacecraft Attitude Dynamics*. Toronto: Wiley, 1986.

[17] C. I. Byrnes, A. Isidori, and J. C. Willems, "Passivity, feedback equivalence, and global stabilization of minimum phase nonlinear systems," *IEEE Trans. Automat. Contr.*, vol. 36, no. 11, pp. 1228–1240, 1991.

[18] M. Vidyasagar, *Nonlinear Systems Analysis*, 2nd ed. Englewood Cliffs, NJ: Prentice-Hall, 1993.

[19] J. LaSalle and Z. Artstein, "The stability of dynamical systems," in *SIAM Regional Conference Series in Applied Mathematics*. Philadelphia: SIAM, 1976, vol. 25.

[20] C. J. Damaren and I. Sharf, "Simulation of flexible-link manipulators with inertial and geometric nonlinearities," *ASME J. Dyn. Syst., Meas., Contr.*, vol. 117, pp. 74–87, Mar. 1995.

[21] I. Sharf and C. J. Damaren, "Simulation of flexible-link manipulators: Basis functions and nonlinear terms in the motion equations," in *Proc. 1992 IEEE Int. Conf. Robotics and Automation*, Nice, France, May, 1992, pp. 1956–1962.

High-Resolution Beam Forming for Ultrasonic Arrays

P. Webb and C. Wykes

***Abstract*—Array processing techniques are common in radar, sonar, and medical ultrasound. However, little work has been reported on the use of array processing with airborne ultrasound. This paper describes the application of array beam forming to airborne ultrasound. It also introduces a processing method which allows the separation between receiving elements to be increased above the traditional $\lambda/2$ limitation. This has the effect of increasing the resolution significantly above that normally expected from traditional array processing methods. A full evaluation of the method is given, a full error analysis of the resulting system is provided, and a comprehensive set of results are presented. The angular and longitudinal resolution of the improved beam former are also derived.**

I. Introduction

If robot systems are to be provided with greater levels of autonomy then they require a detailed knowledge of their surrounding environment. This knowledge may either be preprogrammed or obtained dynamically from sensor systems. One of the most common sensing techniques used for this purpose is ultrasound. The success of this technique has often been limited by the available transducers. The majority of airborne ultrasonic systems have relied on the Polaroid transducer. This is manufactured by the Polaroid Corporation for use as a camera range finder [1]–[4]. A major limitation of this transducer is its limited beam-width ($\approx 30°$) which prevents the construction of phased arrays.

The application of array processing to radar, sonar and medical ultrasound is extensively documented [5]–[7]. Less work has been reported on the application of array processing techniques to airborne ultrasound. Some work has been reported in limited detail by Kay [8]. A system using 16 microphones has also been successfully demonstrated by Horiguchi [9]. The size of the microphones used here meant the spacing between microphones was above the traditional $\lambda/2$ limitation [5], resulting in grating lobes and therefore a limited unambiguous angle of view. A system for use on a mobile robot has also been developed by Seagar *et al.* [10] but this has only limited resolution because of the separation of the elements. Peremans *et al.* [11] used a cluster of three sensors. This system detects the

Manuscript received April 29, 1994; revised February 27, 1995. This work was supported by the United Kingdom Science and Engineering Research Council.

P. Webb is with the Department of Mechanical and Manufacturing Engineering, De Montfort University, The Gateway, Leicester, LE1 9BH, U.K.

C. Wykes is with the Department of Manufacturing Engineering and Operations Management, University of Nottingham, University Park, Nottingham, NG7 2RD, U.K.

Publisher Item Identifier S 1042-296X(96)00494-0.

1042–296X/96$05.00 © 1996 IEEE